Long-term effect of climate change on groundwater recharge in the Grand Est region of France

Ionel Haidu, Mărgărit-Mircea Nistor

Long-term effect of climate change on groundwater recharge in the Grand Est region, France

Ionel Haidu[1], Mărgărit-Mircea Nistor[2,3*]

[1] *Laboratory LOTERR, EA-7304, University of Lorraine, 57045 Metz, France*
[2]*National Institute for Economic Research "Costin C. Kiritescu" of the Romanian Academy/Centre for Mountain Economy (CE-MONT), Romania*
[3]*Department of Hydrogeology, Earthresearch Company, Cluj-Napoca, Romania*

**Corresponding author e-mail: renddel@yahoo.com*

Abstract. Groundwater recharge depends generally on precipitation. In this paper, a GIS procedure was applied to assess the climate change effect on groundwater recharge in the Grand Est region, France. The analysis comprises high-resolution climate models, which reflect the long-term climatological regime. The hydrological properties include aquifers, land cover, and terrain morphology data, which were used to develop the potential infiltration map of the study area. Two parameters, the De Martonne Aridity Index and the effective precipitation, were combined into 5 X 5 matrix to assess the climate change effect on groundwater recharge during past (1990s), present (2020s) and future periods (2050s). The present and future intense aridization and the depletion of the effective precipitation (below 650 mm) reveal the negative effects of climate change on aquifers recharge in the Grand Est region. The areas with high and very high climate effects will increase in the 2020s and 2050s. These areas extend mainly in the western, north-central, and north-eastern parts of the region occupying the Rhine, Aube, and Marne Valleys. The medium effect could be found in the central, southern, and north-western parts, while the low impact on groundwater recharge was verified in the north-western and south-eastern parts of the region. The area with low effects of climate change extends mostly in the Vosges and Ardennes Mountains. These findings contribute to the long-term hydrogeological studies in the Grand Est region.

Keywords: aquifers; effective precipitation; De Martonne Aridity Index; actual crop evapotranspiration.

1. Introduction

Over the last decades, numerous problems related to climate change and environment occurred (IPCC, 2001; Jiménez Cisneros *et al*., 2014). Most of these problems are coming from the climate warming (Haeberli *et al*., 1999) at global level and in several regions (Čenčur Curk *et al*., 2014; Cheval *et al*., 2017). IPCC (2001), Stocks *et al*. (1998), Shaver *et al*. (2000), Stavig *et al*. (2005), The Canadian Centre for Climate Modelling (2014) claimed the increases of mean air temperature and decreases of precipitation amounts in different regions of the world. In Europe, the southern and south-eastern regions are facing reductions of precipitation and waters recharge, especially for the current period (2020s) and the mid-century (2050s) (Čenčur Curk *et al*., 2014; Cheval *et al*., 2017). At high latitudes, the climate warming affected the glaciers and ice masses (Kargel *et al*., 2005; Oerlemans, 2005; Shahgedanova *et al*., 2005; Dong *et al*., 2013; Xie *et al*., 2013; Elfarrak *et al*., 2014), while in the temperate zones and tropics, the climate variation and anthropic factors have major impact on the agriculture, landscape and hydrology. Moreover, the natural and semi-natural areas are likely more susceptible to experience the negative impact due to climate change (Nistor

This article has been accepted for publication and undergone full peer review but has not been through the copyediting, typesetting, pagination and proofreading process, which may lead to differences between this version and the Version of Record. Please cite this article as doi: 10.1002/met.1796

and Mîndrescu, 2017). These areas include forests, shrub and/or herbaceous vegetation associations, and open spaces with little or no vegetation (Kosztra et al., 2017). Due to the increasing of mean air temperature, the groundwater temperature rises and the associated dissolved solutions may induce a low quality to groundwater (Taylor and Stefan, 2009; Figura *et al*., 2011; Kløve *et al*., 2012; Haldorsen *et al*., 2012; Kløve *et al*., 2014; Furtuna et al. 2018).

The negative impact of climate change on surface waters and groundwater resources was observed worldwide. Negative impact on groundwater due to climate change was observed by using the water table measurements and by monitoring the spring discharge (Aguilera and Murillo, 2009; Jiménez Cisneros *et al*., 2014). Čenčur Curk *et al*. (2014) indicated the areas with high impact of climate change on the groundwater vulnerability in the South-East of Europe.

The aim of this work is to assess the climate change effect on effective precipitation in Grand Est region from North-East of France. This is one of the most dynamic regions in Central Europe, with a complex orography and varied climate conditions.

In climatology and hydrology studies, the climate indices are significant due to the ability to characterize the climate regime, humidity-aridity, and continentality-oceanity (Flocas, 1994; Filatov *et al*., 2005; Baltas, 2007). In European regions and not only, the De Mertonne Aridity Index, UNEP Index, Johansson Continentality Index, Pinna Combinative Index, and Kernel Oceanity Index were used for various climate and agricultural investigations (Baltas, 2007; Cheval *et al*., 2017). From these indices, the De Martonne Aridity Index is often used to evaluate the 'aridization – humidity' climate considering the climate data of precipitation and temperature. This index was used at spatial scale for climate characterization and agricultural studies in northern Greece (Baltas, 2007) and in Turkey (Deniz *et al*., 2011).

The effective precipitation is mainly the difference between precipitation amount and evapotranspiration. There are many evapotranspiration methods in the published literature. Penman (1948), Turk (1961), Hargreaves-Samni (1982), Thornthwaite (1948) are some examples of evapotranspiration and evaporation methods used in the hydrological studies. Penman-Montheith method for daily crop evapotranspiration (ETc) was set by Allen *et al*. (1998) and was successfully applied in different regions of the world. For the agricultural studies, Allen (2000), Gowda *et al*. (2008), Prăvălie (2014), Nistor et al. (2018) used the reference evapotranspiration (ETo) and ETc. Actual evapotranspiration (AETo) is mainly used to carry out the water balance calculation (Budyko, 1974). Through Budyko (1974) approach, wide applications of runoff and water surplus determination were conducted (Geritts *et al*. 2009).

Due to the long-term period analysis, Thornthwaite (1948) calculated the ETo and Budyko (1974) calculated the actual evapotranspiration. In addition to the assessment of the land cover evapotranspiration, we adapted the Nistor and Mîndrescu (2017) methodology. They used crop coefficient (Kc) to calculate the ETc and AETc. The adapted version of the NISTOR-CEGW method was applied to determine the long-term climate change effect on groundwater recharge at spatial scale, in the Grand Est region. Climate models, land cover scenarios, terrain morphology, and aquifers composition were analysed by Geographical Information Systems (GIS).

2. Study area

The Grand Est region is located in the north-eastern part of France (Figure 1). Central, northern, southern, and eastern parts of the Grand Est region are the elevated areas, with the Vosges Mountains the south-east. Rhine, Aube, and Marne are the main rivers, which cross the study area

(Vergnes and Habets, 2018). The largest valleys and low lands of the region spread out along these rivers.

The Grand Est region has temperate climate, with precipitation regime of 500-2000 mm/year and higher than 2000 mm in the Vosges mountains (Thierion *et al*., 2012). The mean annual temperature varies from 4 to 10 °C. According to the Koppen-Geiger climate classification, the region is included in the Cfb class, indicating fully humid warm temperate climate with warm summers (Kottek *et al*., 2006).

Vegetation type and land use pattern are in line with the relief and climate conditions of the region. As shown in Supplementary material 1, the land cover of Grand Est region indicates the western part of the region as more agricultural for 2000, 2012, and 2040 in comparison with the western part, which is composed predominantly of different types of forests. Artificial areas are sparsely distributed in the territory, with expectation of urban lands extension for 2040. The implication of land cover typology for evapotranspiration and variety of precipitation control the different recharge amount of groundwater in the Grand Est region.

3. Materials and methods

3.1. Data base

3.1.1. Climate data

The mean monthly air temperature and mean monthly precipitation climate models for 30 years: 1990s (1961-1990), 2020s (2011-2040), and 2050s (2041-2070) were considered for this study. The climate models used here cover the area of Europe and were performed by Andreas Hamann (Hamann *et al*., 2013), from Alberta University, Canada. In the construction models, homogenized data from 1961-1990 (baseline) were considered.

The observed data contain surface observations, accounting for about 1644 stations for temperature (647 for minimum monthly temperature, 344 for mean monthly temperature, and 653 for maximum monthly temperature). These values were quality verified for inhomogeneities (New *et al*., 1998) and used for the construction of grid climatological models at finer resolution (0.5° lat. X 0.5° long.). Approximately 1333 meteorological stations have been used for the precipitation gridded data. These datasets were elaborated in the CRU TS 2.1 project (Mitchell and Jones, 2005) and are available for public and research purposes (http://www.cru.uea.ac.uk/).

The baseline models for the 1990s and future precipitation models of the 2020s and 2050s periods were performed using the Parameter Regression of Independent Slopes Model (PRISM). The temperature models of the same periods include the ANUSplin interpolation method. An emission of Representative Concentration Pathway (RCP) 4.5 was considered for this study, which suggests a moderate climate change for the mid-century, with global predicts of +1.4°C (±0.5).

The final product of the climate models resulted as an ensemble average of 15 AOGCMs related to the CMIP5 multi-model dataset following the IPCC Assessment Report 5 (2013). The ensemble average of 15 AOGCMs, which compose the CMIP5 multi-model, includes CanESM2, CCSM4, INM-CM4, ACCESS1.0, HadGEM2-ES, MRI-CGCM3, IPSL-CM5A-MR, CNRM-CM5, MIROC-ESM, MIROC5, CSIRO Mk 3.6, CESM1-CAM5, MPI-ESM-LR, GFDL-CM3, and GISS-E2R climate models.

The false pixels at the boundaries of low-resolution AOGCM grid cells were corrected using a bilinear interpolation to the anomaly grids prior to overlay. Instead of bias correction, we have applied a Change Factor (CF) method in the raw GCM outputs. The methodology of the models are

in line with the Daly *et al*. (2006) approach and it is explained in detail by Hamann and Wang (2005), Mbogga *et al*. (2009), Wang *et al*. (2016), Dezsi *et al.* (2018). The ClimateEU v4.63 software package was used to perform the climate data models. This software is available on the website (http://tinyurl.com/ClimateEU) and follows the procedure of Hamann *et al*. (2013).

3.1.2. Aquifers data

The main types of aquifers were defined accordingly to the geological compositions and International Hydrogeological Map of Europe (IHME) (Supplementary material 2a) (BGR and UNESCO, 2013). In the Grand Est region, the geology is composed of jointed and karstified limestones, shales, sandstones, conglomerates, mars and clays, and plutonic rocks (Supplementary material 2b). BGR and UNESCO (2013) indicate six types of aquifer productivity. Celico (1988) and Civita (2005) proposed the Potential Infiltration Coefficient (PIC) considering the rocks that composed the aquifer (Supplementary material 3). The significance of the infiltration coefficients in the hydrogeology and groundwater vulnerability calculation is mentioned by Čenčur Curk *et al*. (2014), Nistor *et al*. (2018).

3.1.3. Terrain data

The Digital Elevation Model (DEM) of the Grand Est region shows altitudes varying from 51 m to 1298 m, with the highest values in the Vosges Mountains (Supplementary material 4a). The topography of the region has major implications in the slopes gradient, water flow, and infiltration. The infiltration process is controlled by the lithology and morphology of the terrain. Nistor *et al*. (2018) developed the potential infiltration map model using the ratio between PIC and slope angle (normalized values). The meaning of the concept is based on the reasoning that where the PIC is higher and the slope angle is lower, the infiltration values will be higher. In this study, the DEM of the Grand Est territory served to generate the slope angle map (Supplementary material 4b). This method was applied in the groundwater survey from the Carpathian Mountains (Nistor *et al*., 2018). The mathematical operations were computed on raster grid data in the ArcGIS environment. Figure 3 illustrates the potential infiltration map of the Grand Est region.

3.1.4. Land cover data

Three land cover datasets were used in this study, which refer to CORINE Land Cover database for 2000 and 2012, available on the Copernicus Land Monitoring Services (2012) (http://land.copernicus.eu/) (Supplementary material 1a and b). For the 2040 period, there were used the Hercules models obtained by Schulp *et al*. (2015) in the "Sustainable futures for Europe's HERitage in CULtural landscapES" project (Supplementary material 1c). The land cover projections consider the potential future threats to cultural landscapes and include globalization, demography, and change processes (Schulp *et al*., 2015). In the land cover mapping, the cultural landscapes such as landscape patterns, landscape structure and intensity of land use, cultural significance were included into the "Landscape Character Index". In addition, the "polarization of land use" is based on land abandonment in some places and intense agriculture in other places, which trigger the current changes in cultural landscapes (Gellrich and Zimmermann, 2007; Kuemmerle *et al*., 2008; Navarro and Pereira, 2012; Verburg *et al*., 2010).

Four scenarios (A1, A2, B1, and B2) of future land use changes for 2040 were carried out based on fourteen trajectories in the land trend changes (Schulp *et al*. 2015). These trajectories include the

forestry, agriculture, and urbanization. Scenario A1 focusses on economic growth at global level with increases of the growth of food. In this scenario, the weak regulation on land use change, declining tropical forest areas, and a fully liberalized CAP were considered (Lotze-Campen *et al*., 2013). In Scenario A2, the modest economic growth and no change in the CAP were used. For the Scenario B1, slow growth of food and food demand and modest bioenergy demand were the main differences in comparison with others scenarios. In Scenario B2, the fragmented world with modest economic growth was considered, with no change in the CAP and modest bioenergy demand (Lotze-Campen *et al*., 2013).

In this study, Scenario A1 was chosen since the poor regulation on land use change is predominant and may have major negative environmental impact. Moreover, Nistor and Mîndrescu (2017) argued that Scenario A1 had significant implications at regional scale for the evapotranspiration increase.

The outputs are the raster data of land cover called the 'Hercules models' and are available on the website (http://www.hercules-landscapes.eu/). The land cover raster data were set at 1 X 1 km spatial resolution to be in line with the climate data. This resolution is often used in regional studies.

3.2. De Martonne Aridity Index

The De Martonne Aridity Index is very useful for the climate characterization and moisture evaluation at local scale (Deniz *et al*., 2011). This index was proposed by De Martonne (1925, 1926) and is often used in the climatological and agricultural studies (Zambakas, 1992). Due to its importance, the De Martonne Aridity Index (Eq. (1)) is used for temporal and spatial analyses in various regions of the world (Baltas, 2007).

$$I_{DM} = \frac{PP}{T+10} \quad (1)$$

where

PP annual mean precipitation [mm]

T annual mean air temperature [°C]

Table 1 shows the climate types divided according to De Martonne (1925).

3.3. Evapotranspiration and water availability

3.3.1. Reference evapotranspiration (ETo)

Based on the grid of temperature and precipitation monthly data, the monthly ETo and further annual ETo were calculated using the Thornthwaite (1948) method (Eq. (2)).

$$ETo = 16\left(\frac{10T_i}{I}\right)^{\alpha} \quad (2)$$

where:

ETo monthly reference evapotranspiration [mm]

T_i average monthly temperature [°C], ETo = 0 if the mean temperature < 0

I heat index (Eq.(3))

α complex function of heat index (Eq. (4))

This approach is common for the climate and hydrological studies, especially for the long-term periods (Čenčur Curk *et al*., 2014). Multiplying the ETo by Kc, the ETc could be found (Eq. (2)).

$$I = \sum_{i=1}^{12} \left(\frac{T_i}{5}\right)^{1.514} \quad (3)$$

where:

T_i monthly air temperature

$$\alpha = 6.75 \times 10^{-7} I^3 - 7.71 \times 10^{-5} I^2 + 1.7912 \times 10^{-2} I + 0.49239 \quad (4)$$

where:

I annual heat index

In order to calculate the ETc (Eq.(5)) at spatial scale, Kc values were assigned to each land cover type.

$$\text{Annual ETc} = \text{annual ETo} \times \text{annual Kc} \quad (5)$$

where:

ETc crop evapotranspiration [mm]

ETo reference evapotranspiration [mm]

Kc crop coefficient [dimensionless]

Allen *et al*. (1998) provided the seasonal Kc values for crops in 'FAO Irrigation and Drainage Paper 56'. Grimmond and Oke (1999) carried out the Kc for the urban areas of the temperate zone. In this paper, we agree with the annual Kc values (Tables 2 and 3) used by Nistor and Mîndrescu (2017) and Nistor (2018) (Supplementary material 5). They calculated the annual values of Kc from the ratio of the annual ETc carried out with four seasons with specific seasonal Kc and the annual ETo. For the future land cover projection, we chose Scenario A1 because it seemed most unfavourable from the evapotranspiration (high amount) point of view at spatial scale.

3.3.2. Actual crop evapotranspiration (AETc)

We have applied the Budyko approach (Eq. (6)) (Budyko, 1974).

$$\frac{AETc}{PP} = \left[\left(\varphi \tan \frac{1}{\varphi}\right)(1 - \exp^{-\varphi})\right]^{0.5} \quad (6)$$

where:

AETc actual land cover evapotranspiration [mm]

PP total annual precipitation [mm]

φ aridity index (Eq. (7))

$$\varphi = \frac{\mathrm{ETc}}{\mathrm{PP}} \quad (7)$$

This method is useful for the water balance calculation and indicates if the heat energy is quite high to produce the evaporation from the precipitation amount (Gerrits *et al*., 2009; Cencur Curk *et al*., 2014). The procedure implies the aridity index determination and AETc calculation for an annual period. Here, we incorporated the ETc instead of ETo to find the aridity index (Eq. (6)). Thus, the land cover evapotranspiration is included in the AETc method.

3.3.3. Water availability

In order to determine the water availability during the 1990s, 2020s, and 2050s, climate models and land cover were used to calculate AETc. From the difference between annual precipitation and AETc, the maps of water availability were carried out (Eq. (7)). All calculations were completed in the ArcGIS 10.5 environment at high spatial resolution (1 km^2).

$$\mathrm{WA} = \mathrm{PP} - \mathrm{AETc} \quad (8)$$

where:

WA water availability [mm]

PP total annual precipitation [mm]

AETc actual land cover evapotranspiration [mm]

3.4. Effective precipitation

Based on the terrain lithology and morphology, a certain amount of water availability infiltrates the soil and it is supposed to recharge the aquifers. According to the rainfall intensity and saturation of the soil, the infiltration process takes different times for different typology of rocks. Russo *et al*. (2015) assessed the regional suitability for managed aquifer recharge using GIS and novel approaches for datasets combination, including surface and subsurface hydrologic properties and conditions. The main data used in their methodology is based on geology, soil infiltration capacity, land use, topographic slope, and measured infiltration. Russo *et al*. (2015) classified the layers using a relative scale of 1 to 5 in base of three methods: knowledge of field properties, GIS natural breaks considering the distribution of property values, and raw data operations. In South Italy, Cianflone *et al*. (2015) developed a GIS procedure to estimate the potential recharge of aquifers in the Sibari Plain. Based on the previous hydrogeological studies (Celico, 1988), they assigned a value of PIC to each type of lithology. Multiplying the effective rainfall by PIC and correction factor, Cianflone *et al*. (2015) calculated the effective infiltration.

Here, we determined the effective precipitation by multiplying the water availability with potential infiltration map (Eq. (9)).

$$\mathrm{EPP} = \mathrm{WA} \times \mathrm{PIM} \quad (9)$$

where:

EPP Effective precipitation [mm]

WA Water availability [mm]

PIM Potential infiltration map [dimensionless]

Since this is a study over a long period, it is difficult to account for the time variable for the infiltration process. In this study, the normalized potential infiltration map was used, divided in ten equal classes from 0.1 to 1. This procedure was applied to avoid the calculations with very small values which occur in the infiltration map (bellow 0.1) and are not realistic, especially for the artefacts cells. Moreover, through this method, the results are in line with the hydrogeological studies. This type of normalization was used by Gardi *et al*. (2010) to avoid the division by 0.

3.5. Matrix method to assess the climate effect on groundwater recharge

This approach was adapted after the NISTOR–CEGW matrix method, which combines the De Martonne Aridity Index and effective precipitation to assess the effect of climate change on groundwater resources (Nistor and Mîndrescu, 2017). In addition, we used potential infiltration map to obtain the effective precipitation.

Five classes of climate effect were defined for the final layers of the De Martonne Aridity Index and effective precipitation: very low, low, medium, high, and very high. The De Martonne Aridity Index was set according to the climate classification of this index from the extremely humid class to the Mediterranean class. For the Grand Est region, the semi-dry and dry climates were not identified. The effective precipitation was classified into five categories, as follows: 0 – 50 mm, 51 – 100 mm, 101 – 300 mm, 301 – 500 mm, and above 500 mm.

In order to assess the climate change effect on groundwater recharge, we used the 5 x 5 matrix method to combine the De Martonne Aridity Index and effective precipitation. The meaning of the matrix (Figure 3) suggests that the areas with low values of the De Martonne Aridity Index and areas with low values of effective precipitation represent areas susceptible to climate change effect on groundwater recharge.

4. Results

4.1. Variation of climate over 1990s, 2020s, 2050s

The climate parameters of temperature, precipitation, and ETo were analysed at spatial scale during 1961-1990 (1990s), 2011-2040 (2020s), and 2041-2070 (2050s). Considering these metrics, advanced calculations regarding the AETc, water availability, and effective precipitation were completed for the three temporal windows in the Grand Est region. Overall, the climate change impact on the evapotranspiration and effective precipitation in Grand Est region from North-East of France would seem to have a negative impact, mainly for the future period.

Considering the baseline climate models (1990s), the mean annual temperature for the past period ranged from 4.1 °C to 10.7 °C (Figure 4a). For the same period, the mean annual precipitation values ranged from 568 mm to 2414 mm in the Grand Est region (Figure 4d) while the annual ETo values ranged from 392 mm to 548 mm (Figure 4g). The areas with high mean annual temperature (above 10 °C) and high annual ETo (above 500 mm) overlap the Rhine, Marne, and Aube Valleys. In these areas, the annual precipitation shows lower values (below 600 mm). In the

Vosges and Ardennes Mountains, the mean annual temperatures and annual ETo are lower (below 6°C and below 400 mm, respectively).

Consistent increases in the maximum mean annual temperature (+2.5 °C) between the 1990s and the 2050s could be observed in the climate models (Figures 4a and c), with high impact in the western and eastern parts of the Grand Est region. Precipitation pattern for the future period indicates no significant changes (Figures 4e and f), while the annual ETo shows increases up to 631 mm and up to 657 mm for the 2020s (Figures 4h and i), with significant impact on the whole territory, especially in the low lands (e.g. Rhine, Marne, Aube valleys). These values have negative influence on the groundwater recharge due to the decrease in the water availability and effective precipitation.

4.2. Variation of the De Martonne Aridity Index

The spatial distribution of the De Martonne Aridity Index in the Grand Est region was computed based on climate models and using GIS techniques. During the 1990s, the index values range from 28.57 to 154.91 (Figure 5a), while during the 2020s, the De Martonne Aridity Index ranges from 26.74 to 140.31 (Figure 5c) and during the 2050s this index ranges from 24.65 to 133.32 (Figure 5e). The higher values of the index (above 55) denote an extremely humid climate mainly in the south-eastern part, where the Vosges Mountains spread out. The high values were identified also in few locations from the south-central and north-western parts of the Grand Est. The major part of the territory is characterized as very humid (values from 35 to 55) and humid (values above 28 and below 35). During the 2020s and 2050s, the De Martonne Aridity Index decreases, indicating a gradual aridization for the 21st century. Thus, in 2020s some locations in the western and south-eastern parts appear as semi-humid, while in the 2050s the semi-humid class is more pronounced in western and eastern parts of the region. In this period, the areas with very humid and extremely humid classes of the De Martonne Aridity Index decreased and the semi-humid class expanded in area. This detail indicates a climate change negative effect in the region.

4.3. Variation of evapotranspiration and water availability

By applying the presented methodology, the spatial distribution of annual ETc and annual AETc in the Grand Est region were found. Thus, during the 1990s, the annual ETc ranges from 93 mm to 777 mm, while in the near-term period of 2020s the annual ETc ranges from 102 mm to 892 mm and in the 2050s period, the annual ETc ranges from 138 mm to 873 mm. The high values (above 700 mm) of annual ETc during the 1990s could be observed in the central and southern parts of the Grand Est region (Supplementary material 6a), especially in the Meuse and Haute Marne provinces. The lowest values (below 300 mm) of annual ETc are mainly identified in the artificial areas and sparsely in the north-western, southern, and north-eastern parts. In the years 2020s and 2050s the annual ETc has high values in the centre, east, and south-west of the Grand Est region, while lower values were identified in few locations, where the major built up area was located (Supplementary material 6c and e).

The annual AETc ranges during the 1990s from 92 mm to 650 mm (Supplementary material 6b) showing high values (above 600 mm) in the central and south-eastern parts of the region. The lower values (below 300 mm) spread in the western, northern, and north-eastern, but also in the central parts of the Grand Est region, where the artificial areas extend. During the 2020s and 2050s periods, the annual AETc indicates values between 101 mm and 738 mm (2020s), 136 mm and 723 mm

(2050s), respectively. The high values occupy more territory in the future periods than for the past period showing high values in central, south-eastern, south-central, and north-western parts (Supplementary material 6d and f). The lower values could be found in few of the southern, western, central, and eastern parts of the Grand Est region.

Water availability variation for 1990s period in the Grand Est region is shown in Figure 5b. The values range from 123 mm to 1973 mm indicating high values (above 1000 mm) in the south-central, south-eastern, and north-western areas. Thus, the Vosges Mountains represent the extended area with high water availability in the Grand Est region. The lower values (below 300 mm) of water availability were depicted in the western, eastern, and north-eastern parts of the region, mainly in the Marne Valley, Aube Valley, and Rhine Valley. Low values of water availability could be found also in the north-central and south-western parts of the study area. The results of the future models show a large territory with lower water availability (below 200 mm) than in the past period. Figures 5d and f illustrate the water availability for the 2020s and 2050s. The most affected lands are Rhine, Marne and Aube Valleys, which spread out in the western and eastern parts of the region.

4.4. Variation of effective precipitation

The effective precipitation in the Grand Est region ranges from 12 mm to 637 mm (1990s) indicating high values in the Bas Rhin and Ardennes provinces of the region (Figure 6a). The lower values (below 100 mm) could be found in the most part of the territory, except the Vosges Mountains and Rhine Valley, but also in several locations from the west, centre, south-centre, and north-west of the Grand Est region. In the future, decrease in the effective precipitation values is expected in the study area. Thus, values which range from 10 mm to about 600 mm will be experienced in the Grand Est region during the 2020s and 2050s, with significant changes at spatial scale mainly in the central and north-central parts (Figure 6b and c). In these areas, lower values (below 100 mm) were identified. The west and east are facing less effective precipitation, while the Vosges Mountains record lower values of the effective precipitation (below 100 mm). In the mountainous areas, effective precipitation ranges from 100 mm to 200 mm, while few territories from north and north-west appear with high effective precipitation values (over 600 mm). On the one hand, the compacted rocks with low permeability (shales, plutonic rocks) and low PIC (about 0.1) influence these results in the mountains areas. Moreover, Vosges and Ardennes Mountains were classified as non-aquiferous rocks (BGR and UNESCO, 2013). On the other hand, in the areas with high PIC (above 0.8), the aquifers composed by gravels and sands are affected by climate change due to low values of water availability. The formations that represent highly productive aquifers (calcarenites and sands, chalkstones, limestone, conglomerates, sands, and gravels) experience low effective precipitation due to decrease in water availability.

4.5. Climate change effect on groundwater recharge

Over the past period (1990s), the climate change effect on groundwater recharge is higher in the western, north-central, north-eastern, and eastern parts of the Grand Est region (Figure 7a). Current (2020s) and future (2050s) periods experience appropriate pattern of the high effect and, in addition, very high effects were identified in the western and eastern parts. The territories of Marne, Haut Rhin, and Bas Rhin provinces are the most affected by climate change (Figure 7b and c). The medium effect of climate spreads in the central, south-central and north-western parts of the Grand Est region (1990s). Low and very low effects of climate change on groundwater recharge were

found in the northern, north-western, south-central, and south-eastern parts of the region. These areas overlap the Vosges Mountains, Ardennes, and the high lands of Haute Marne, Vosges, and South of Haut Rhine provinces. The western and eastern parts, but also the north-central part of the Grand Est region, experience greater effect of climate change during the 2020s and 2050s.

Analysing the hydrogeological system of the Grand Est region, the findings reflect the effect of climate change on both the external agents (temperature, precipitation, orography, and land cover) and the internal factor (geology). The main concern regarding the climate change and groundwater resources in the study area indicates that the geology of the study area plays an important role in the groundwater recharge. In addition, through the De Martonne Aridity Index, the aridity variation at spatial scale suggests that the Grand Est region is susceptible to aridization over the current century. These findings, combined with the effective precipitation, contribute to clear understanding of the hydrology of the area. Moreover, the De Martonne Aridity Index shows a switch of the climate class from very humid to humid in the provinces of Mouse, Moselle, and the northern part of Meurthe et Moeselle. Because of this, these territories may record less water availability and long draught periods during the summer season.

5. Discussion

The goal of the present work is to assess the climate change effect on effective precipitation in the Grand Est region using a spatial-temporal method. Considering the 30 years climate data models over 1961-2070, the territory of the studied region experiences the high pressure of the climate change. The western, north-central, north-eastern, and eastern parts of the Grand Est region faced the high effect of climate on groundwater recharge during the 1990s (Figure 7a) and the future period of the 2020s and 2050s appears to be under much negative influence of climate change. Thus, the results indicate lands with very high impact of climate change on groundwater in the Rhine Valley (Figure 7b) during the 2020s and an increase of the impact is obviously observed for the 2050s in the western and eastern parts (Figure 6c), in the Rhine Valley especially in Bas Rhine and Haut Rhine provinces and Marne province. These findings are mainly in direct relation with the increase of mean annual temperature in the region, influencing the annual ETo.

As consequences, these climate outcomes combining with the high values of the annual Kc (around 1.01-1.42) in the western and eastern parts contribute to the higher annual ETc. Arable lands and forestry areas contribute much to the annual ETc and AETc increase. The annual AETc includes the precipitation pattern and our results are closer to the real situation of evapotranspiration. For instance, even if the Vosges Mountains territory has a lower annual temperature and lower annual ETo than other parts of the Grand Est region, the higher values of annual precipitation induce the high values of AETc in this part of the region. However, the mountainous lands of the region indicate a reduced area with high values of effective precipitation (above 1000 mm).

Our findings concur with other results from other regions using an appropriate methodology. After applying the same procedure, Nistor and Mîndrescu (2017) found the annual ETc values of 1147 mm, 1100 mm, and 1084 mm during the 1990s, 2020s, and 2050s in the Emilia-Romagna region from Italy. Nistor and Mîndrescu (2017) calculated the AETc values of 817 mm, 762 mm, and 751 mm and the water availability values of 1973 mm, 1989 mm, and 1810 mm during the 1990s, 2020s, and 2050s for the same region. Cheval *et al*. (2017) indicate values up to 165 of the De Martonne Aridity Index in South-Eastern Europe for the 1961-2050 period. The results achieved in this paper and other studies are very close, the differences are mainly due to the geographical

position of other regions and climatic database used by other authors. The presented methodology has high reliability on climatic and hydrological studies at regional scale, for long-term period. Through this method, the preliminary assessment of climate effect on effective precipitation could be carried out and further investigations by in-situ monitoring may complement the survey at local scale. However, using the NISTOR-CEGW approach, the main territories affected by climate change over the mid-century in the Grand Est region were identified including also the terrain data, geology of the area, and aquifer productivity maps.

The maps of annual ETc, AETc, and effective precipitation are influenced by the land cover pattern. The future scenario for 2040 does not present a detailed list of some land classes, e.g. forest and urban areas. Thus, the differences between broad-leaved forest and coniferous forest, but also between many artificial areas were not included for Hercules models. We chose a value of 0.26 for built up areas in 2040, which meant an average of all artificial areas presented in the CLC 2000 and 2012, so the results of future period were not much influenced by the annual Kc rather than by future climatic conditions. These inconveniences may influence the results to a minimal extent.

6. Conclusions

The climate change effect on groundwater recharge in Grand Est region was assessed through the adapted NISTOR-CEGW method. High-resolution climate models, aquifers, terrain morphology and land cover data served for the analysis during the 1990s, 2020, and 2050s. In order to estimate the climate change effect, the De Martonne Aridity Index and effective precipitation were calculated at spatial scale and inserted into the 5 x 5 matrix. The output of matrix inference indicates five effect classes. During the 1990s, the findings show high effect of climate on groundwater recharge in major part of the region. Moreover, during the 2020s and 2050s, the very high effect was identified in the western and eastern parts of the Grand Est region. The low and very low impact of climate change on groundwater resources overlap with the highlands of the Vosges Mountains and the Ardennes Mountains, but these areas experience less territory with low and very low effect during the 2020s and 2050s. The medium effect was identified much in the north-eastern and south-central parts of the region.

In the territories composed by karstified limestones, gravel and sands, which are highly productive aquifers, the climate change has high impact during all three periods. In addition, the usage of arable land in these problematic areas contributes to the negative effect on groundwater and surface water resources in the Grand Est region. For the current century, more irrigation systems and a good water management plan could improve the quality of the environment and water resources.

The adaptation of the NISTOR–CEGW method indicates a good performance at regional scale of the Grand Est territory. The results are in line with the published literature, which suggests that the methodology was applied correctly. Moreover, we present a regional study that focuses on the long-term period and the findings may indicate future perspectives for scientists in climatology, hydrogeology, and environmental fields. For a better functionality and management of the Grand Est region, our maps and results represent important tools mainly for the regional administration and policymakers. Under the recent climate change, the groundwater resources in the Grand Est region require more attention and adequate action plans should be considered.

Acknowledgements

This research was supported by Centre de recherche en Géographie, LOTTER-EA7304, Université de Lorraine, Metz in the framework of the project RECRET - AAP-2017-TELL-PR19. The authors would like to thank Andreas Hamann from Alberta University for the climate models data. We address many thanks to the anonymous reviewers, which contribute to the manuscript improvement!

References

Aguilera, H., and Murillo, J.M. (2009) The effect of possible climate change on natural groundwater recharge based on a simple model: a study of four karstic aquifers in SE Spain. *Environmental Geology* 57(5), 963–974.

Allen, R.G., Pereira, L.S., Raes, D., and Smith, M. (1998) *Crop Evapotranspiration: Guidelines for Computing Crop Water Requirements.* FAO Irrigation and Drainage Paper 56. FAO: Rome; pp. 300.

Allen, R.G. (2000) Using the FAO-56 dual crop coefficient method over an irrigated region as part of an evapotranspiration intercomparison study. *Journal of Hydrology* 229, 27–41.

Baltas, E. (2007) Spatial distribution of climatic indices in northern Greece. *Meteorological Applications* 14, 69–78.

BGR and UNESCO. (2013) *International Hydrogeological Map of Europe (IHME1500) 1:1,500,000*. International Association of Hydrogeologists. http://www.bgr.bund.de/ihme1500/.

Budyko, M.I. (1974) *Climate and life*. Academic Press, New York, USA, pp. 508.

Čenčur Curk, B., Cheval, S., Vrhovnik, P., Verbovšek, T., Herrnegger, M., Nachtnebel, H.P., Marjanović, P., Siegel, H., Gerhardt, E., Hochbichler, E., Koeck, R., Kuschnig, G., Senoner, T., Wesemann, J., Hochleitner, M., Žvab Rožič, P., Brenčič, M., Zupančič, N., Bračič Železnik, B., Perger, L., Tahy, A., Tornay, E.B., Simonffy, Z., Bogardi, I., Crăciunescu, A., Bilea, I.C., Vică, P., Onuţu, I., Panaitescu, C., Constandache, C., Bilanici, A., Dumitrescu, A., Baciu, M., Breza, T., Marin, L., Draghici, C., Stoica, C., Bobeva, A., Trichkov, L., Pandeva, D., Spiridonov, V., Ilcheva, I., Nikolova, K., Balabanova, S., Soupilas, A., Thomas, S., Zambetoglou, K., Papatolios, K., Michailidis, S., Michalopoloy, C., Vafeiadis, M., Marcaccio, M., Errigo, D., Ferri, D., Zinoni, F., Corsini, A., Ronchetti, F., Nistor, M.M., Borgatti, L., Cervi, F., Petronici, F., Dimkić, D., Matić, B., Pejović, D., Lukić, V., Stefanović, M., Durić, D., Marjanović, M., Milovanović, M., Boreli-Zdravković, D., Mitrović, G., Milenković, N., Stevanović, Z., and Milanović, S. (2014) *CC-WARE Mitigating Vulnerability of Water Resources under Climate Change*. WP3 - Vulnerability of Water Resources in SEE, Report Version 5. URL: http://www.ccware.eu/output-documentation/output-wp3.html.

Celico, P. (1988) *Prospezioni idrogeologiche.* Liguori Ed., vol.II, pp. 521. (in Italian)

Cheval S, Dumitrescu A, Barsan MV. 2017. Variability of the aridity in the South-Eastern Europe over 1961–2050. *Catena* 151, 74–86.

Cianflone, G., Dominici, R., and Viscomi, A. (2015) Potential recharge estimation of the Sibari plain aquifers (Southern Italy) through a new GIS procedure. *Geographia Technica* 10(1), 8-18.

Civita, M. (2005) *Idrogeologia applicata ed ambientale*. CEA, Milano, Italy. (in Italian)

Copernicus Land Monitoring Services. (2012) *CORINE Land Cover of Europe*. URL: http://land.copernicus.eu/ (accessed 21 July 2016).

Daly, C., Halbleib, M., Smith, J.I., Gibson, W.P., Doggett, M.K., Taylor, G.H., and Curtis J. (2006) Physiographically-sensitive mapping of temperature and precipitation across the conterminous United States. *International Journal of Climatology* 28, 2031–2064.

De Martonne, E. (1925) *Traité Géographie. Physique: 3 tomes*. Max leclcrc and H. Bourrclier, proprietors of Librairic Armard Colin: Paris. (in French)

De Martonne, E. (1926) A new climatological function: the aridity index. *La Météorologie* 2, 449–458. (in French)

Deniz A, Toros H, and Incecik S. (2011) Spatial variations of climate indices in Turkey. *International Journal of Climatology* 31, 394–403.

Dezsi, Șt., Mîndrescu, M., Petrea, D., Rai, K.P., Hamann, A., and Nistor, M.M. (2018) High-resolution projections of evapotranspiration and water availability for Europe under climate change. *International Journal of Climatology* 38(10), 3832–3841. https://doi.org/10.1002/joc.5537.

Dong, P., Wang, C., and Ding, J. (2013) Estimating glacier volume loss used remotely sensed images, digital elevation data, and GIS modelling. *International Journal of Remote Sensing* 34(24), 8881–8892.

Elfarrak, H., Hakdaoui, M., and Fikri, A. (2014) Development of Vulnerability through the DRASTIC Method and Geographic Information System (GIS) (Case Groundwater of Berrchid), Morocco. *Journal of Geographic Information System* 6, 45–58.

Figura, S., Livingstone, D.M., Hoehn, E., and Kipfer, R. (2011) Regime shift in groundwater temperature triggered by the Arctic Oscillation. *Geophysical Research Letters* 38(L23401), 1–5.

Filatov, N., Salo, Y., and Nazarova, L. (2005) *Effect of climate variability on natural water bodies in Northwest Russia*. In 15th International Northern Research Basins Symposium and Workshop. Luleå to Kvikkjokk, Sweden, 31–40.

Flocas, A.A. (1994) *Courses of Meteorology and Climatology*. Ziti Publications: Thessaloniki. (in Greek)

Furtuna, P., Haidu, I., and Maier, N. (2018) Synoptic Processes Generating Windthrows. A Case Study in the Apuseni Mountains (Romania). *Geographia Technica* 13(2), 52-61.

Gardi, C., Bosco, C., Rusco, E., and Montanerella, L. (2010) An analysis of the Land Use Sustainability Index (LUSI) at territorial scale based on Corine Land Cover. *Management of Environmental Quality: An International Journal* 21(5), 680-694.

Gellrich, M., and Zimmermann, N.E., (2007) Investigating the regional-scale pattern of agricultural land abandonment in the Swiss mountains: A spatial statistical modelling approach. *Landscape and Urban Planning* 79: 65–76. doi:10.1016/j.landurbplan.2006.03.004.

Gerrits, A.M.J., Savenije, H.H.G., Veling, E.J.M., and Pfister L. (2009) Analytical derivation of the Budyko curve based on rainfall characteristics and a simple evaporation model. *Water Resources Research* 45(W04403), 1–15, DOI: 10.1029/2008WR007308.

Gowda, P.H., Chavez, J.L., Colaizzi, P.D., Evett, S.R., Howell, T.A., and Tolk, J.A. (2008) ET mapping for agricultural water management: present status and challenges. *Irrigation Science* 26(3), 223–237.

Grimmond, C.S.B., and Oke, T.R. (1999) *Evapotranspiration rates in urban areas, Impacts of Urban Growth on SurfaceWater and Groundwater Quality*. Proceedings of IUGG 99 Symposium HSS. Birmingham, July 1999.

Haeberli, W.R., Frauenfelder, R., Hoelzle, M., and Maisch, M. (1999) On rates and acceleration trends of global glacier mass changes. *Geografiska Annaler, Series A, Physical Geography* 81A, 585– 595.

Haldorsen, S., Heim, M., and van der Ploeg M. (2012) *Impacts of Climate Change on Groundwater in Permafrost Areas - Case Study from Svalbard, Norway*. pp. 323–340. In: Treidel, H., Martin-Bordes, J.J., Gurdak, J.J. (Eds.), Climate Change Effects on Groundwater Resources: A Global Synthesis of Findings and Recommendations. International Association of Hydrogeologists (IAH). International Contributions to Hydrogeology. Taylor & Francis Publishing, pp. 414.

Hamann, A., and Wang, T.L. (2005) Models of climatic normals for genecology and climate change studies in British Columbia. *Agricultural and Forest Meteorology* 128, 211–221.

Hamann, A., Wang, T., Spittlehouse, D.L., and Murdock, T.Q. (2013) A comprehensive, high-resolution database of historical and projected climate surfaces for western North America. *Bulletin of the American Meteorological Society* 94, 1307–1309.

Hargreaves, G.A., and Samni, Z.A. (1982) Estimation of potential evapotranspiration. *J. Irrig. Drain. Div., Proc. Amer. Soc. Civ. Eng*. 108, 223–230.

Kosztra, B., Büttner, G., Hazeu, G., and Arnold, S. (2017) Updated CLC illustrated nomenclature guidelines. European Topic Centre on Urban, land and soil systems. Published by Environment Agency Austria, Wien, Austria.

IPCC. (2001) *Climate change 2001: the scientific basis*. In: Houghton JT, Ding Y, Griggs DJ, Noguer M, van der Linden PJ, Dai X. (Eds), Contribution of Working Group I to the Third Assessment Report of the Intergovernmental Panel on Climate Change. Cambridge University Press: Cambridge and New York, New York, pp. 881.

IPCC. (2013) *Summary for Policymakers.* In: Stocker TF, Qin D, Plattner G-K, Tignor M, Allen SK, Boschung J, Nauels A, Xia Y, Bex V, Midgley PM. (Eds.), Climate Change 2013: The Physical Science Basis. Contribution of Working Group I to the Fifth Assessment Report of the Intergovernmental Panel on Climate Change. Cambridge University Press, Cambridge, United Kingdom and New York, USA, pp. 1308.

Jiménez Cisneros, B.E., Oki, T., Arnell, N.W., Benito, G., Cogley, J.G., Döll, P., Jiang, T., and Mwakalila, S.S. (2014) *Freshwater resources*. In: Field CB, Barros VR, Dokken DJ, Mach KJ, Mastrandrea MD, Bilir TE, Chatterjee M, Ebi KL, Estrada YO, Genova RC, Girma B, Kissel ES, Levy AN, MacCracken S, Mastrandrea PR, White LL (Eds.), Climate Change 2014: Impacts, Adaptation, and Vulnerability. Part A: Global and Sectoral Aspects. Contribution of Working Group II to the Fifth Assessment Report of the Intergovernmental Panel on Climate Change. Cambridge University Press, Cambridge, United Kingdom and New York, USA, pp. 229–269.

Kargel, J.S., Abrams, M.J., Bishop, M.P., Bush, A., Hamilton, G., Jiskoot, H., Kääb, A., Kieffer, H.H., Lee, E.M., Paul, F., Rau, F., Raup, B., Shroder, J.F., Soltesz, D., Stainforth, S., Stearns, L., and Wessels, R. (2005) Multispectral imaging contributions to global land ice measurements from space. *Remote Sensing of Environment* 99(1), 187–219.

Kløve, B., Ala-Aho, P., Okkonen, J., and Rossi, P. (2012) *Possible Effects of Climate Change on Hydrogeological Systems: Results From Research on Esker Aquifers in Northern Finland*, pp. 305–322. In: Treidel H, Martin-Bordes JJ, Gurdak JJ (Eds.), Climate Change Effects on Groundwater Resources: A Global Synthesis of Findings and Recommendations. International Association of Hydrogeologists (IAH). International Contributions to Hydrogeology. Taylor & Francis Publishing, pp. 414.

Kløve, B., Ala-Aho, P., Bertrand, G., Gurdak, J.J., Kupfersberger, H., Kværner, J., Muotka, T., Mykrä, H., Preda, E., Rossi, P., Bertacchi Uvo, C., Velasco, C., and Pulido-Velazquez. M. (2014) Climate change impacts on groundwater and dependent ecosystems. *Journal of Hydrology* 518, 250–266.

Kottek, M., Grieser, J., Beck, C., Rudolf, B., and Rubel, F. (2006) World Map of the Köppen-Geiger climate classification updated. *Meteorologische Zeitschrift* 15(3), 259–263.

Kuemmerle, T., Hostert, P., Radeloff, V.C., van der Linden, S., Perzanowski, K., and Kruhlov, I. (2008) Cross-border Comparison of Post-socialist Farmland Abandonment in the Carpathians. *Ecosystems* 11, 614–628. doi:10.1007/s10021-008-9146-z.

Mitchell, T.D., and Jones, P.D. (2005) An improved method of constructing a database of monthly climate observations and associated high-resolution grids. *International Journal of Climatology* 25, 693–712.

Mbogga, M.S., Hamann, A., and Wang, T. (2009) Historical and projected climate data for natural resource management in western Canada. *Agricultural and Forest Meteorology* 149, 881–890.

Navarro, L.M., and Pereira, H.M. (2012) Rewilding Abandoned Landscapes in Europe. Ecosystems 15, 900–912. doi:10.1007/s10021-012-9558-7.

New, M., Hulme, M., and Jones, P. (1998) Representing Twentieth-Century Space–Time Climate Variability. Part I: Development of a 1961–90 Mean Monthly Terrestrial Climatology. *Journal of Climate* 12, 829–856.

Nistor, M.M., and Mîndrescu, M. (2017) Climate change effect on groundwater resources in Emilia-Romagna region: An improved assessment through NISTOR-CEGW method. *Quaternary International*. https://doi.org/10.1016/j.quaint.2017.11.018.

Nistor, M.M. (2018) Projection of annual crop coefficients in Italy based on climate models and land cover data. *Geographia Technica* 13(2), 97-113.

Nistor, M.M., Man, T.C., Benzaghta, M.A., Nedumpallile Vasu, N., Dezsi, S¸ and Kizza, R. (2018) Land cover and temperature implications for the seasonal evapotranspiration in Europe. *Geographia Technica*, 13(1), 85-108.

Nistor, M.M., Nicula, A.S., Cervi, F., Man, T.C., Irimuş, I.A., and Surdu, I. (2018) Groundwater vulnerability GIS models in the Carpathian Mountains under climate and land cover changes. *Applied Ecology and Environmental Research* 16(4), 5095-5116.

Oerlemans, J. (2005) Extracting a Climate Signal from 169 Glacier Records. *Science* 308, 675–677.

Penman, H.L. (1948) Natural evaporation from open water, bare soil and grass. *Proceedings of the Royal Society of London. Series A, Mathematical and Physical Sciences* 193(1032), 120-145.

Prăvălie, R. (2014) Analysis of temperature, precipitation and potential evapotranspiration trends in southern Oltenia in the context of climate change. *Geographia Technica* 9(2), 68–84.

Russo, T.A., Fisher, A.T., and Lockwood, B.S. (2015) Assessment of Managed Aquifer Recharge Site Suitability Using a GIS and Modeling. *Groundwater* 53(3), 389–400.

Schulp, C.J.E., Tieskens, K.F., Sturck, J., Fuchs, R., van der Zanden, E.H., Schrammeijer, E., and Verburg, P.H. (2015) *EU scale analysis of future cultural landscape dynamics*. Report no. 1, WP 5 Fine - and broad-scale modelling of future landscapes.

Shahgedanova, M., Stokes, C.R., Gurney, S.D., and Popovnin, V. (2005) Interactions between mass balance, atmospheric circulation, and recent climate change on the Djankuat Glacier, Caucasus Mountains, Russia. *Journal of Geophysical Research* 110(D16107), 1–12.

Shaver, G.R., Canadell, J., Chapin III. F.S., Gurevitch, J., Harte, J., Henry, G. et al. (2000) Global warming and terrestrial ecosystems: a conceptual framework for analysis. *BioScience* 50(10), 871–882.

Stavig, L., Collins, L., Hager, C., Herring, M., Brown, E., and Locklar, E. (2005) The effects of climate change on Cordova, Alaska on the Prince William Sound. *Alaska Tsunami Papers, The National Ocean Sciences Bowl*. https://seagrant.uaf.edu/nosb/papers/2005/cordova-nurds.html (accessed 23 April 2014).

Stocks, B.J., Fosberg, M.A., Lynham, T.J., Mearns, L., Wotton, B.M., Yang, Q. et al. (1998) Climate change and forest fire potential in Russian and Canadian boreal forests. *Clim. Change* 38, 1–13.

Taylor, C.A., and Stefan, H.G. (2009) Shallow groundwater temperature response to climate change and urbanization. *Journal of Hydrology* 375 (3–4), 601–612.

The Canadian Centre for Climate Modelling and Analysis. (2014) The first generation coupled global climate model publishing web. URL: http://www.ec.gc.ca/ccmac-cccma/default.asp?lang=En&n= 540909E4-1 (accessed 20 March 2015).

Thierion, C., Longuevergne, L., Habets, F., Ledoux, E., Ackerer, P., Majdalani, S., Leblois, E., Lecluse, S., Martin, E., Queguiner, S., and Viennot, P. (2012) Assessing the water balance of the Upper Rhine Graben hydrosystem. *Journal of Hydrology* 424-425, 68–83.

Thornthwaite, C.W. (1948) An approach toward a rational classification of climate. *Geographical Review* 38, 55–94.

Turc, L. (1961) Estimation of irrigation water requirement, potential evapotranspiration: a simple climatic formula evolved up to date. *Annals of Agronomy* 12, 13-49.

Verburg, P.H., van Berkel, D.B., van Doorn, A.M., van Eupen, M., and van den Heiligenberg, H.A.R.M. (2010) Trajectories of land use change in Europe: a model-based exploration of rural futures. *Landscape Ecology* 25, 217–232.

Vergnes, J.P., and Habets, F. (2018) Impact of river water levels on the simulation of stream–aquifer exchanges over the Upper Rhine alluvial aquifer (France/Germany). *Hydrogeology Journal*, https://doi.org/10.1007/s10040-018-1788-0.

Wang, T., Hamann, A., Spittlehouse, D.L., and Carroll, C. (2016) Locally downscaled and spatially customizable climate data for historical and future periods for North America. *PLoS One* 11, e0156720.

Xie, X., Li, Y.X., Li, R., Zhang, Y., Huo, Y., Bao, Y., and Shen S. (2013) Hyperspectral characteristics and growth monitoring of rice (Oryza sativa) under asymmetric warming. *International Journal of Remote Sensing* 34(23), 8449–8462.

Zambakas, J. (1992) *General Climatology.* Department of Geology, National and Kapodistrian University of Athens: Athens. (in Greek)

Figure captions

Figure 1. Location of the Grand Est region in France and physical map of the region.

Figure 2. Potential infiltration map of the Grand Est region. Note: Potential infiltration map was calculated as ratio of potential infiltration coefficient and normalization slope layer (radian degrees).

Figure 3. Inference matrix used to assess climate change effects on groundwater resources in the Grand Est region.

Figure 4. Spatial distribution of mean annual air temperature (TT), annual precipitation (PP), and reference evapotranspiration (ETo) in the Grand Est region. (a) TT in 1990s. (b) TT in 2020s. (c) TT in 2050s. (d) PP in 1990s. (e) PP in 2020s. (f) PP in 2050s. (g) ETo in 1990s. (h) ETo in 2020s. (i) ETo in 2050s.

Figure 5. Spatial distribution of the De Martonne Aridity Index and water availability in the Grand Est region. (a) De Martonne Aridity Index in 1990s. (b) Water availability in 1990s. (c) De Martonne Aridity Index in 2020s. (d) Water availability in 2020s. (e) De Martonne Aridity Index in 2050s. (f) Water availability in 2050s.

Figure 6. Spatial distribution of effective precipitation in the Grand Est region for different periods: (a). 1990s, (b). 2020s, and (c). 2050s.

Figure 7. Climate change effect on groundwater recharge in the Grand Est region. (a). 1990s, (b). 2020s, and (c). 2050s.

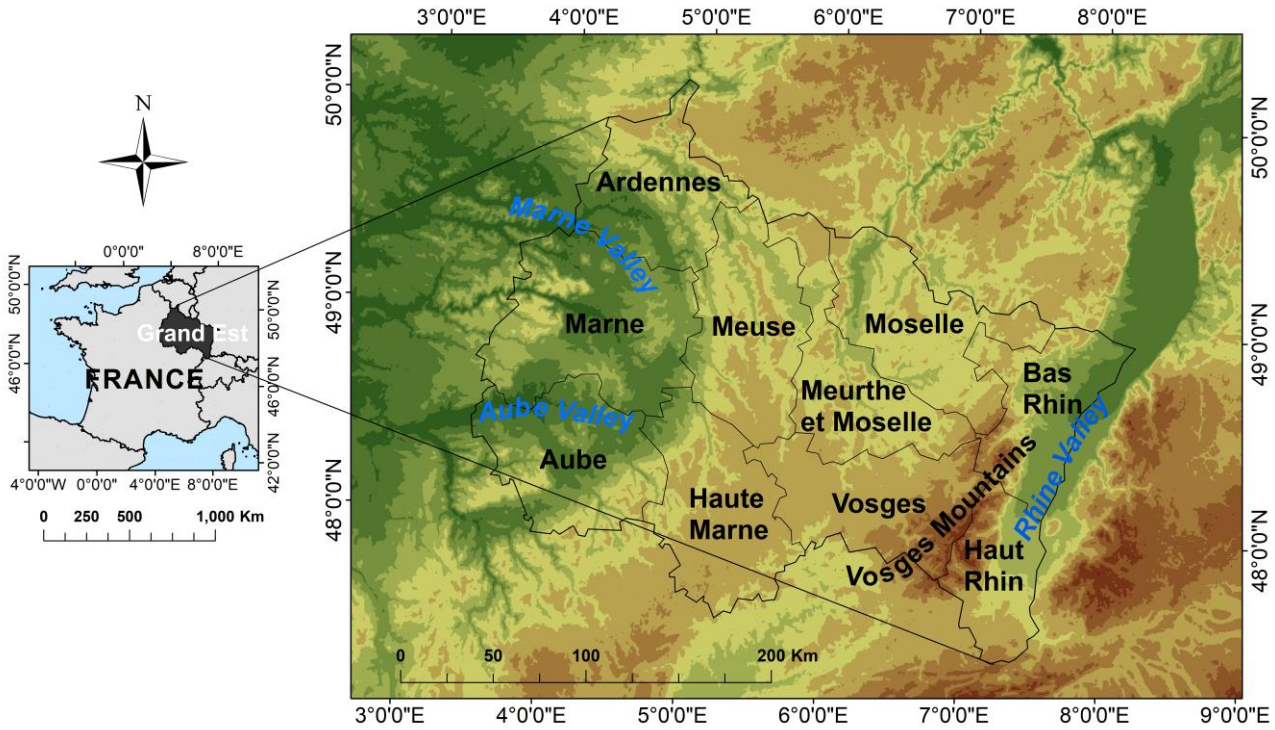

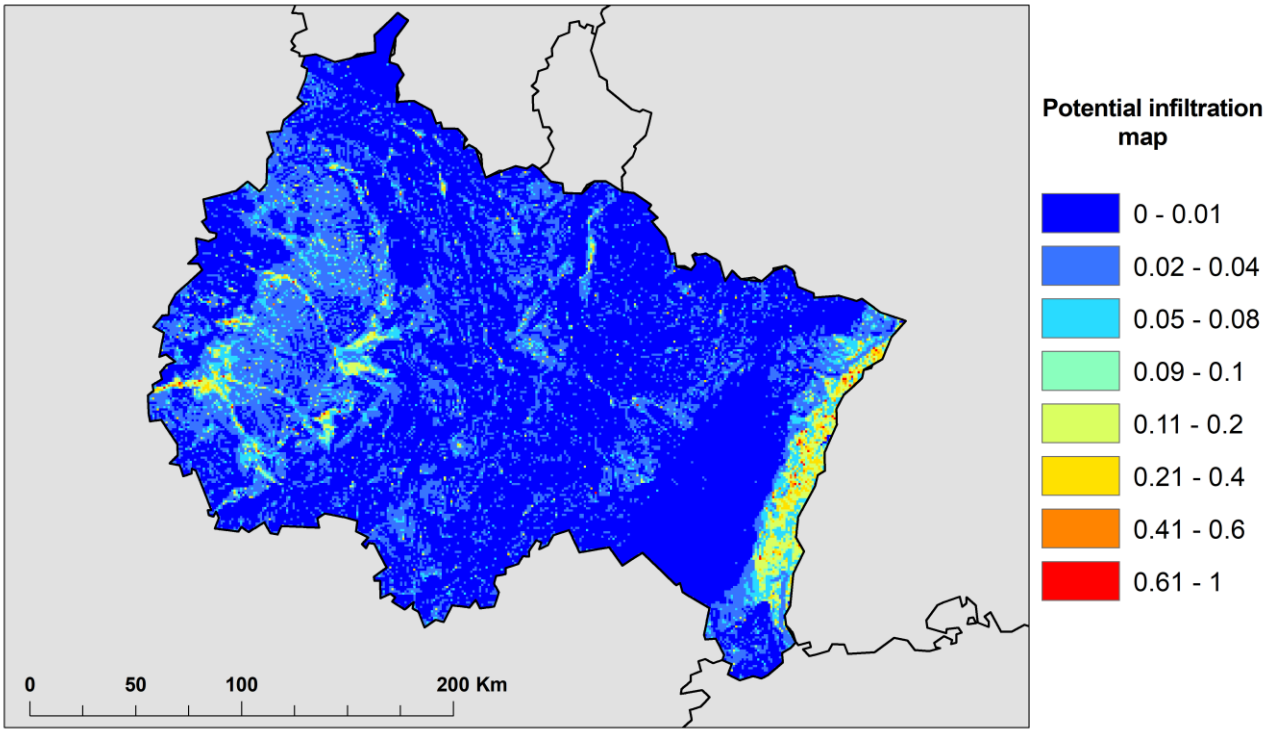

Climate type De Martonne Index		Effect
Extremely humid	> 55	Very low
Very humid	35 ≤ IDM ≤ 55	Low
Humid	28 ≤ IDM < 35	Medium
Semi-humid	24 ≤ IDM < 28	High
Mediterranean	20 ≤ IDM < 24	Very high

Effective precipitation (mm)				
0 - 50	51 - 100	101 - 300	301 - 500	> 500
Very high	High	Medium	Low	Very low

Medium	Low	Low	Very low	Very low
High	Medium	Low	Low	Very low
High	High	Medium	Low	Low
Very high	High	High	Medium	Low
Very high	Very high	High	High	Medium

Climate change effect

Very high	High	Medium	Low	Very low

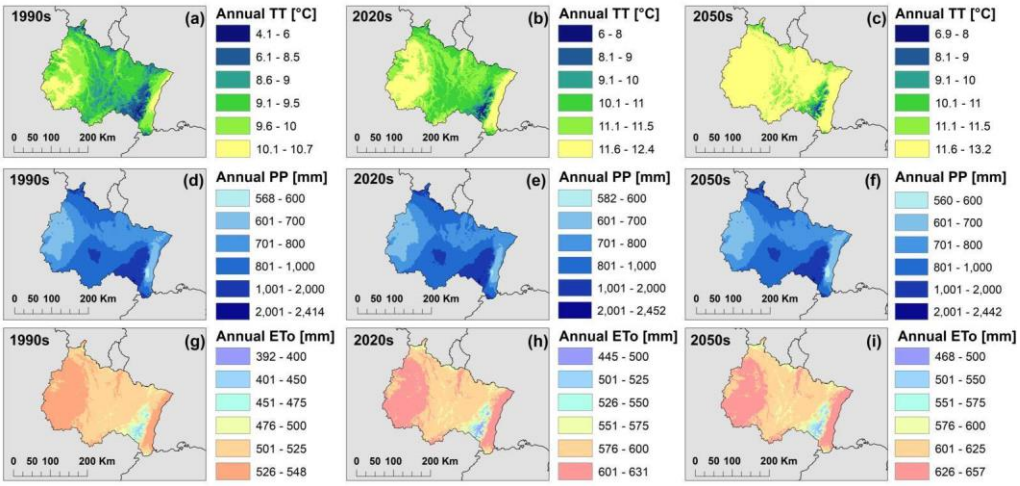

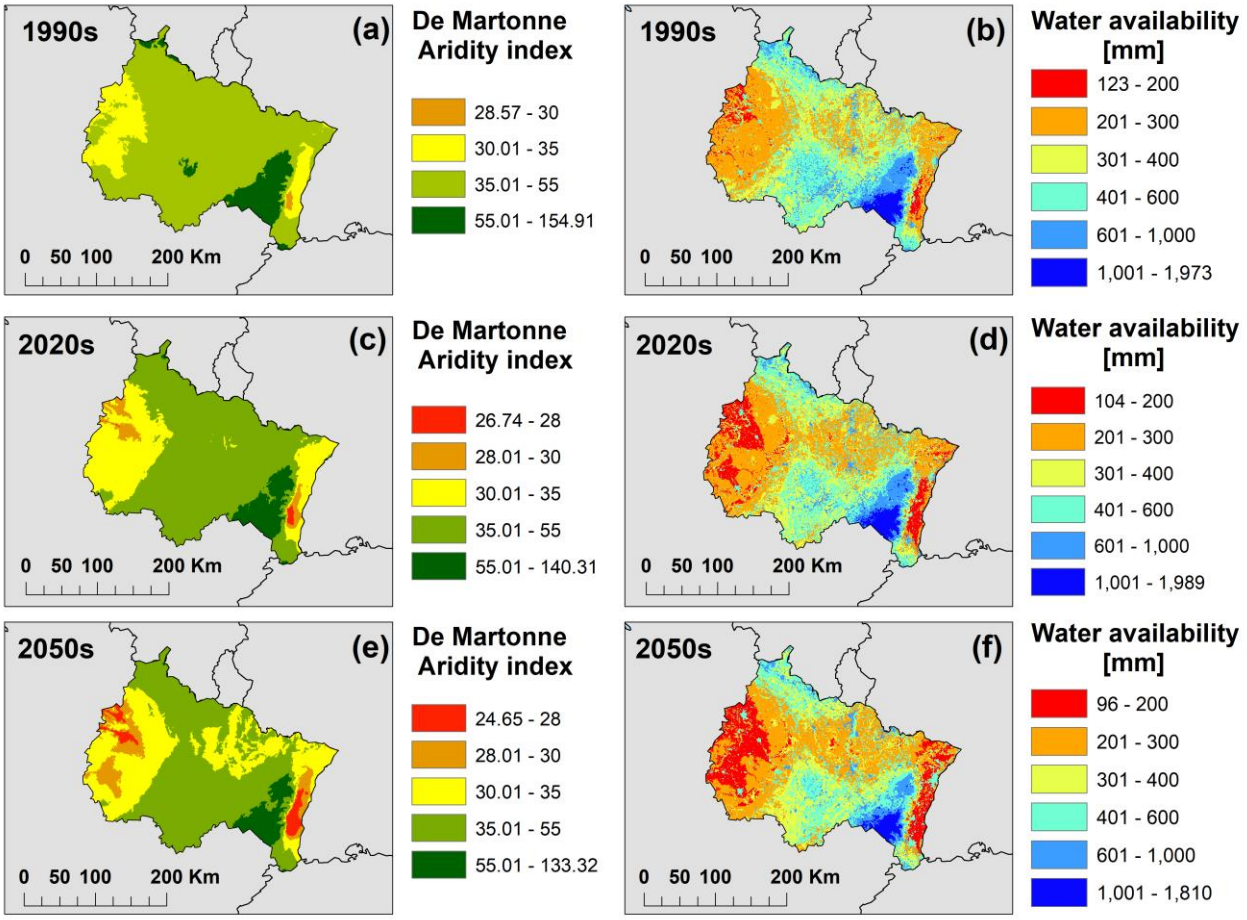

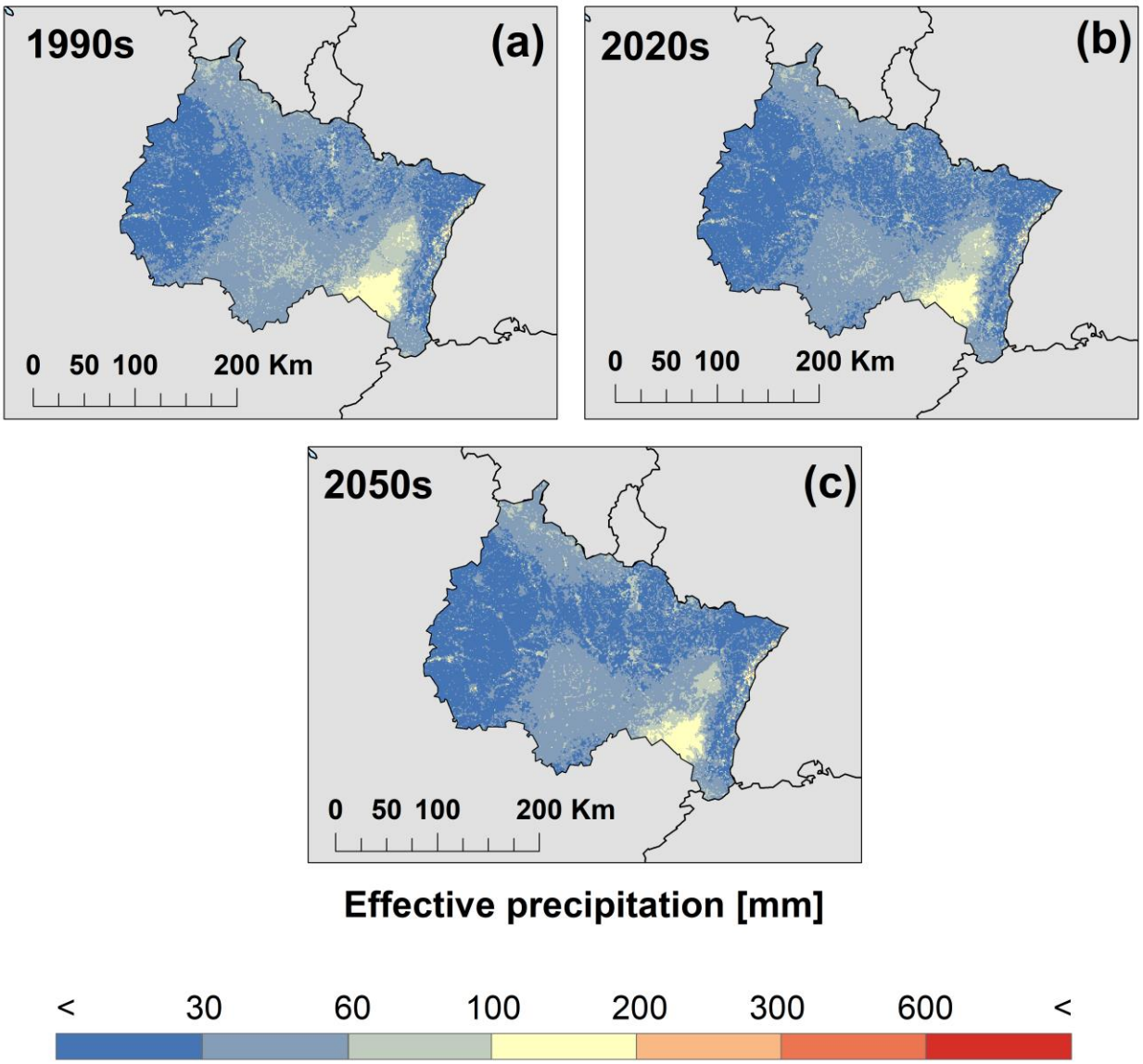

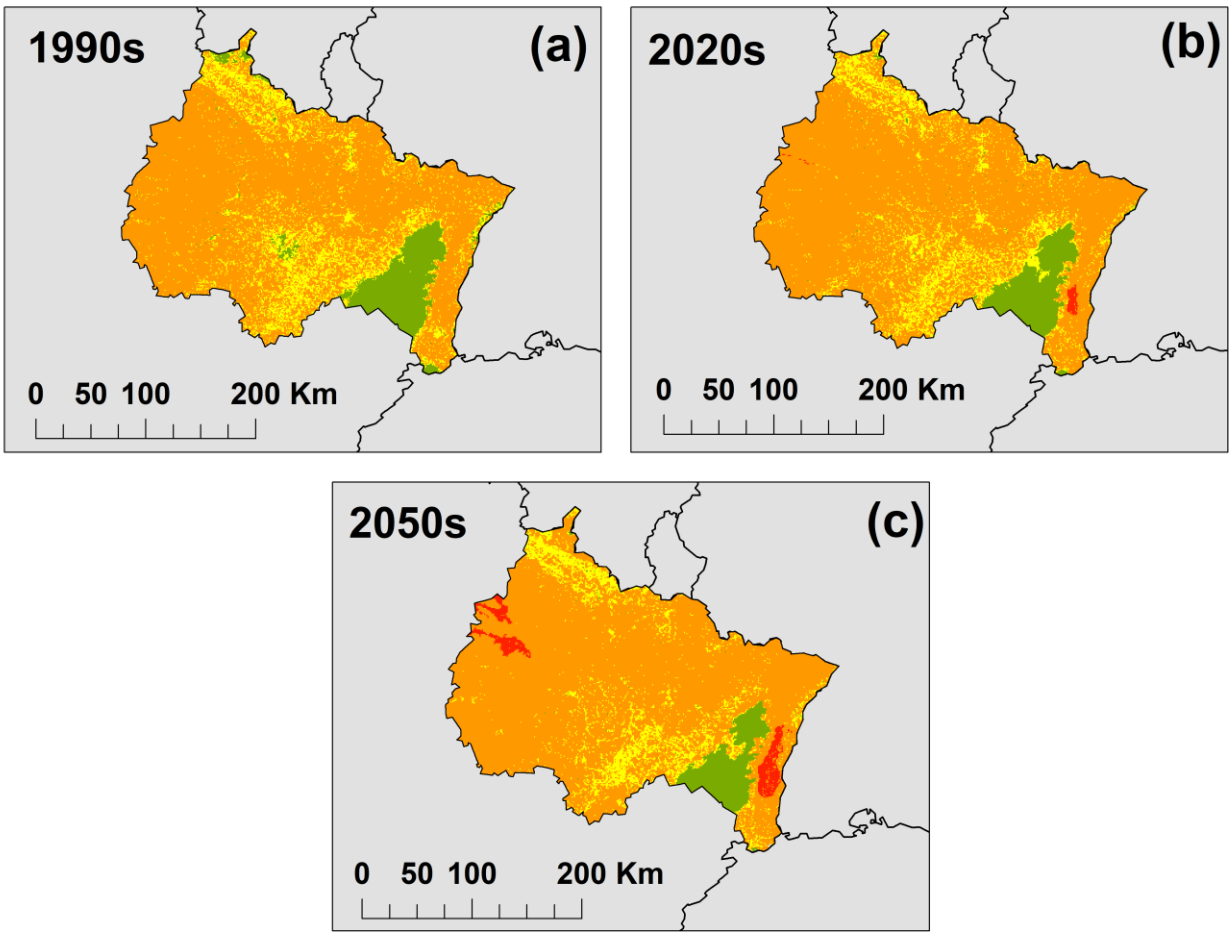

Table 1. Climatic classification of the De Martonne Aridity Index.

Climate types	De Martonne Aridity Index	Precipitation (mm)
Extremely humid	>55	P > 800
Very humid	35 ≤ IDM ≤ 55	700 ≤ P ≤ 800
Humid	28 ≤ IDM < 35	600 ≤ P < 700
Semi-humid	24 ≤ IDM < 28	50 ≤ P < 600
Mediterranean	20 ≤ IDM < 24	400 ≤ P < 500
Semi-dry	10 ≤ IDM < 20	200 ≤ P < 400
Dry	< 10	P < 200

Table 2. Corine Land Cover classes and annual Kc for present in Grand Est region.

Corine Land Cover		Kc annual				
CLC code 2012	CLC Description	Kc	Ks	Ku	Kw	Kclc
111	Continous urban fabric	-	-	0.3	-	0.29
112	Discontinuous urban fabric	-	-	0.2	-	0.21
121	Industrial or commercial units	-	-	0.3	-	0.3
122	Road and rail networks and associated land	-	-	0.3	-	0.25
123	Port areas	-	-	0.4	-	0.39
124	Airports	-	-	0.3	-	0.3
131	Mineral extraction sites	-	-	0.3	-	0.26
132	Dump sites	-	-	0.3	-	0.26
133	Construction sites	-	-	0.3	-	0.26
141	Green urban areas	-	-	0.2	-	0.21
142	Sport and leisure facilities	-	-	0.2	-	0.21
211	Non-irrigated arable land	1.14	-	-	-	1.14
212	Permanently irrigated land	1.25	-	-	-	1.25
213	Rice fields	0.94	-	-	-	0.94
221	Vineyards	0.5	-	-	-	0.5
222	Fruit trees and berry plantations	0.68	-	-	-	0.68
223	Olive groves	0.66	-	-	-	0.66
231	Pastures	0.7	-	-	-	0.7
241	Annual crops associated with permanent crops	0.67	-	-	-	0.67
242	Complex cultivation patterns	1.16	-	-	-	1.16
243	Land principally occupied by agriculture, with significant areas of natural vegetation	0.92	-	-	-	0.92
244	Agro-forestry areas	0.92	-	-	-	0.92
311	Broad-leaved forest	1.42	-	-	-	1.42
312	Coniferous forest	1	-	-	-	1
313	Mixed forest	1.33	-	-	-	1.33
321	Natural grasslands	0.97	-	-	-	0.97
322	Moors and heathland	0.92	-	-	-	0.92

323	Sclerophyllous vegetation	0.62	-	-	-	0.62
324	Transitional woodland-shrub	0.83	-	-	-	0.83
331	Beaches, dunes, sands	-	0.23	-	-	0.23
332	Bare rocks	-	0.15	-	-	0.15
333	Sparsely vegetated areas	0.48	-	-	-	0.48
334	Burnt area	-	0.1	-	-	0.1
335	Glaciers and perpetual snow	-	-	-	0.51	0.51
411	Inland marshes	-	-	-	0.45	0.45
412	Peat bogs	-	-	-	0.37	0.37
421	Salt marshes	-	-	-	0.32	0.32
422	Salines	-	0.1	-	-	0.1
423	Intertidal flats	-	-	-	0.64	0.64
511	Water courses	-	-	-	0.63	0.63
512	Water bodies	-	-	-	0.64	0.64
521	Coastal lagoons	-	-	-	0.68	0.68
522	Estuaries	-	-	-	0.62	0.62
523	Sea and ocean	-	-	-	0.74	0.74

Kc - crop coefficient for plants, Ks - evaporation coefficient for bare soils, Ku - crop coefficient for urban areas, Kw - evaporation coefficient for open water, Kclc - crop coefficient for land cover. Source: From Allen et al. (1998); Nistor and Mîndrescu (2017), Nistor (2018)

Table 3. Corine Land Cover classes and annual Kc for future scenarios in Grand Est region.

Corine Land Cover			Kc				
CLC code 2012	CLC projection code	CLC Description	Kc	Ks	Ku	Kw	Kclc
133	0	Built-up area	-	-	0.26	-	0.26
211	1	Arable land (non-irrigated)	1.14	-	-	-	1.14
231	2	Pasture	0.7	-	-	-	0.7
321 and 324	3	Natural and semi-natural vegetation (including Natural grasslands, scrublands, regenerating forest below 2 m, and small forest patches within agricultural landscapes)	0.9	-	-	-	0.9
411	4	Inland wetlands	-	-	-	0.45	0.45
335	5	Glaciers and snow	-	-	-	0.51	0.51
212	6	Irrigated arable land	1.25	-	-	-	1.25
321	7	Recently abandoned arable land (i.e. “long fallow”; includes very extensive farmland not reported in agricultural statistics, herbaceous vegetation, grasses and shrubs below 30 cm)	0.97	-	-	-	0.97
241	8	Permanent crops	0.67	-	-	-	0.67
313	10	Forest	1.33	-	-	-	1.33
333	11	Sparsely vegetated areas	0.48	-	-	-	0.48
331	12	Beaches, dunes and sands	-	0.23	-	-	0.23
422	13	Salines	-	0.1	-	-	0.1
423 and 521	14	Water and coastal flats	-	-	-	0.66	0.66
322	15	Heathland and moorlands	0.92	-	-	-	0.92
231 and 324	16	Recently abandoned pasture land (includes very extensive pasture land not reported in agricultural statistics, grasses and shrubs below 30cm)	0.76	-	-	-	0.76

Kc - crop coefficient for plants, Ks - evaporation coefficient for bare soils, Ku - crop coefficient for urban areas, Kw -

evaporation coefficient for open water, Kclc - crop coefficient for land cover. Source: From Allen et al. (1998); Nistor and Mîndrescu (2017), Nistor (2018).